Journal of Nanobiotechnology

RESEARCH

Open Access

Magnetic vagus nerve stimulation ameliorates contrast-induced acute kidney injury by circulating plasma exosomal miR-365-3p

Tianyu Wu[1†], Wenwu Zhu[2†], Rui Duan[2†], Jianfei Sun[3], Siyuan Bao[3], Kaiyan Chen[4], Bing Han[2*], Yuqiong Chen[5*] and Yao Lu[2*]

Abstract

Background Contrast-induced acute kidney injury (CI-AKI) is manifested by a rapid decline in renal function occurring within 48–72 h in patients exposed to iodinated contrast media (CM). Although intravenous hydration is currently the effective method confirmed to prevent CI-AKI, it has several drawbacks. Some investigations have demonstrated the nephroprotective effects of vagus nerve stimulation (VNS) against kidney ischemia-reperfusion injury, but no direct research has investigated the use of VNS for treating CI-AKI. Additionally, most current VNS treatment applies invasive electrical stimulator implantation, which is largely limited by the complications. Our recent publications introduce the magnetic vagus nerve stimulation (mVNS) system pioneered and successfully used for the treatment of myocardial infarction. However, it remains uncertain whether mVNS can mitigate CI-AKI and its specific underlying mechanisms. Therefore, we herein evaluate the potential therapeutic effects of mVNS on CM-induced nephropathy in rats and explore the underlying mechanisms.

Results mVNS treatment was found to significantly improve the damaged renal function, including the reduction of elevated serum creatinine (Scr), blood urea nitrogen (BUN), and urinary N-acetyl-β-D-glucosaminidase (NAG) with increased urine output. Pathologically, mVNS treatment alleviated the renal tissue structure injury, and suppressed kidney injury molecule-1 (KIM-1) expression and apoptosis in renal tubular epithelial cells. Mechanistically, increased circulating plasma exosomal miR-365-3p after mVNS treatment enhanced the autophagy and reduced CM-induced apoptosis in renal tubular epithelial cells by targeting Ras homolog enriched in brain (Rheb).

Conclusions In summary, we demonstrated that mVNS can improve CI-AKI through enhanced autophagy and apoptosis inhibition, which depended on plasma exosomal miR-365-3p. Our findings highlight the therapeutic

†Tianyu Wu, Wenwu Zhu and Rui Duan contributed equally to this work.

*Correspondence:
Bing Han
hbing777@hotmail.com
Yuqiong Chen
cosmoscyq@163.com
Yao Lu
luyaoyanyan@njmu.edu.cn

Full list of author information is available at the end of the article

potential of mVNS for CI-AKI in clinical practice. However, further research is needed to determine the optimal stimulation parameters to achieve the best therapeutic effects.

Graphical abstract

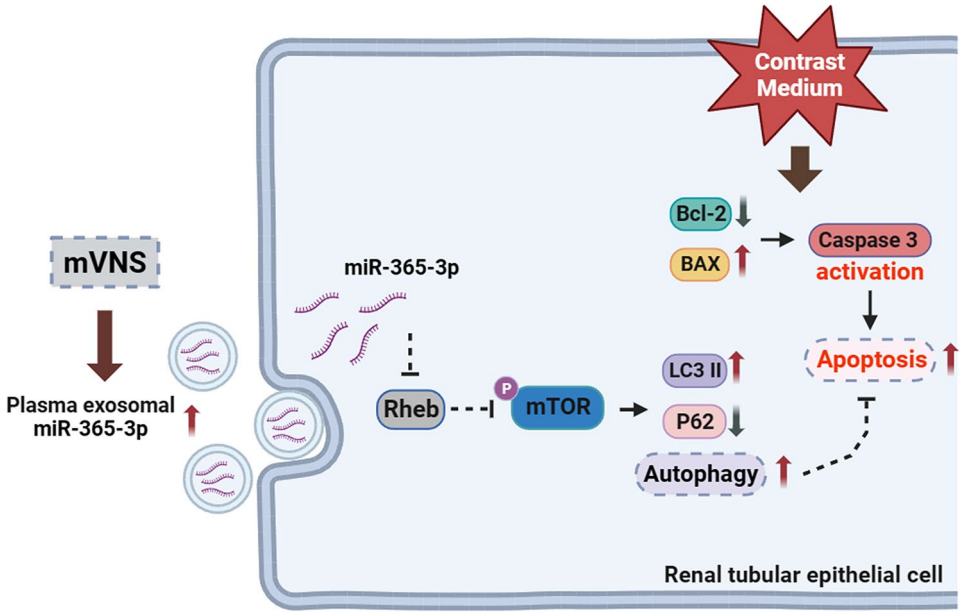

Keywords CI-AKI, mVNS, Exosome, miR-365-3p, Autophagy

Introduction

Contrast-induced acute kidney injury (CI-AKI) is characterized by a rapid and significant impairment of renal function, as indicated by elevated plasma creatinine and/or reduced urine output within 48–72 h in patients receiving contrast media (CM) [1]. According to data from the National Cardiovascular Data Registry (NCDR) Cath-PCI registry, the incidence of CI-AKI in patients undergoing percutaneous coronary intervention (PCI) is between 7% and 8% [2, 3]. Notably, the incidence of CI-AKI surpasses 25% in patients with advanced chronic kidney disease (CKD) undergoing PCI [4]. The molecular mechanisms underlying acute kidney injury (AKI) induced by contrast media primarily stem from its direct cytotoxic effects on renal tubular cells and endothelial cells. This leads to excessive reactive oxygen species (ROS) generation, promoting mitochondrial dysfunction and apoptosis [5, 6]. Additionally, contrast media has indirect effects on severe hemodynamic disorders, contributing to renal medullary hypoxia and, consequently, enhancing ROS formation [7–10]. Although intravenous hydration is currently the only effective method confirmed to prevent CI-AKI [11, 12], it has several drawbacks. Foremost among these is the risk of excessive fluid supply, which may elevate the likelihood of CI-AKI and death in patients with renal dysfunction following PCI surgery [13]. Therefore, there is an urgent need to develop more comprehensive prevention and treatment strategies to reduce the incidence of CI-AKI in clinical settings.

Vagus nerve stimulation (VNS), initially developed for treating epilepsy and refractory depression [14], has found application in managing inflammatory diseases, including rheumatoid arthritis and Crohn's disease [15, 16].While there is currently no direct study on the treatment of CI-AKI with VNS, numerous investigations have demonstrated the nephroprotective effects of VNS against acute kidney injuries related to ischemia-reperfusion [17–19]. This protection is attributed to the activation of the cholinergic anti-inflammatory pathway (CAP), resulting in the suppression of systemic pro-inflammatory cytokines like TNF-α [18, 20–22]. Most current VNS studies involve the invasive electrical stimulator implantation [23]. Unfortunately, this highly invasive neuromodulation approach is largely limited by the complications including battery replacement, wires breakage, infection and venous thrombosis [24]. In our previous research, we have innovatively established a magnetic vagus nerve stimulation (mVNS) system based on the application of an external magnetic field and an injectable hydrogel infused with superparamagnetic iron oxide (SPIO) nanoparticles coated with chitosan-β-glycerophosphate

(CS/β-GP) [25]. Utilizing the mVNS system, we realized the precise and effective stimulation of cervical vagus nerve and further confirmed the safety, and stability of mVNS for treating myocardial ischemic injuries in rats [25, 26]. However, it is not clear whether mVNS can ameliorate CI-AKI, which needs further study.

In addition to its anti-inflammatory effects through CAP, a recent study highlighted that VNS could mitigate the systemic inflammatory response after hemorrhagic shock via exosomes, where VNS treatment altered the proinflammatory protein components of exosomes (Exo) in the post-shock mesenteric lymph [27]. This finding prompts the hypothesis that VNS may have the potential to inhibit CI-AKI by modulating circulating exosomes. Exosomes, nano-sized particles actively released from cells into interstitial space or peripheral circulation, serve as the carriers of signaling molecules such as proteins, microRNAs (miRNAs), and long non-coding RNAs (lncRNAs) to facilitate the communications between cells, tissues and organs [28–30]. MiRNAs are currently recognized as the most abundant contents in exosomes [31, 32]. They typically function by recognizing the specific sites like 3'-untranslated regions (3'-UTRs) on the target mRNAs, leading to mRNA degradation [33–35]. Previous studies have confirmed that vagus nerve activation could regulate the macrophages in spleen via the CAP and exert a renal protective effect [18, 21]. Recent studies have found that microRNA-365-3p (miR-365-3p) is abundant and highly conserved across species [36], and enriched in exosomes derived from macrophages, which has been implicated in the modulation of cancer, inflammatory response and atherosclerosis [37–39]. These results suggest that miR-365-3p may be enriched in exosomes under the influence of mVNS. Interestingly, we observed that mVNS treatment can elevate the levels of exosomal miR-365-3p in plasma. Although multiple studies have demonstrated the involvement of exosomal miRNAs in modulating AKI caused by various etiologies through their regulation of necroptosis, apoptosis, autophagy, and the oxidative stress response [33, 40], it remains unclear whether miR-365-3p participates in these nephroprotective effects. Hence, we hypothesized that mVNS treatment may improve CI-AKI through exosomal miR-365-3p and conducted further investigation to determine the specific mechanisms.

In the present study, our findings indicate that mVNS treatment significantly mitigated CI-AKI by inhibiting apoptosis and enhancing autophagy. Furthermore, we validated that the exosomes derived from rats subjected to mVNS notably alleviated CM-induced renal dysfunction and apoptosis while enhancing autophagy in vivo and in vitro. We identified the overexpression of miR-365-3p within these exosomes, and elucidated its downstream target gene Ras homolog enriched in brain (Rheb) as the key molecules responsible for the nephroprotective effects of mVNS.

Results

Establishment of the magnetic vagus stimulation system and experimental procedures

Figure 1A illustrates the composition of the SPIO-CS/β-GP temperature-sensitive hydrogels (Fig. 1A). Based on our previous reports [25], the SPIO-CS/GP temperature-sensitive hydrogel was successfully synthesized by adding the SPIO nanoparticles (approved by the FDA for clinical use [41]) to the CS/GP system. As shown in Fig. 1B, the SPIO-CS/β-GP hydrogels were injected to the left cervical vagus nerve of rats, which would become solidificated under the body temperature and thus wrap around the vagus tightly. Then left cervical vagus nerve would be stimulated magnetically once the rotating magnet passed by (Fig. 1B). Iohexol, considered as a widely used contrast agent in clinical practice that can directly induce nephrotoxicity in renal tubular epithelial cells [42], was used to induce CI-AKI [6, 43]. Figure 1C exhibited the schematic representation of CI-AKI model establishment and mVNS treatment (Fig. 1C).

mVNS treatment significantly attenuated iohexol-induced kidney injury and improved renal function

To evaluate the renoprotective effect of mVNS against iohexol-induced AKI, rats underwented the magnetic stimulation of left vagus nerve one day before the injection of iohexol. Renal function was assessed by measuring levels of SCr, BUN, NAG, and 24-hour urine output volume. The results showed that iohexol exposure significantly increased the levels of SCr, BUN, NAG and led to the reduction in 24 h-urine volume, while mVNS treatment resulted in a 55% decrease in SCr level and a 45% decrease in BUN level, and also reversed elevated NGA and reduced 24 h-urine output. (Fig. 2A). Furthermore, renal glomerular and tubular structures were examined by hematoxylin-eosin (H&E) and periodic acid-Schiff (PAS) staining. Histological analysis revealed the distinct signs of damage in the CM group, including dilation and disarray of tubular lumina and reduction of tubular epithelial cells, along with the increased expression of kidney injury molecule-1(KIM-1). KIM-1 showed increased abundance in renal tubular epithelial cells after injury and thus served as a biomarker of the severity of kidney injury [44]. Concurrently, the renal tubular injury score correspondingly increased under iohexol treatment. After mVNS treatment, the aforementioned histological changes were significantly attenuated (Fig. 2B and C). These results suggested that mVNS can ameliorate the renal injuries in CI-AKI rats. In addition, TUNEL staining confirmed that mVNS could reduce apoptosis in renal tubular epithelial cells induced by CM (Fig. 2D). Western

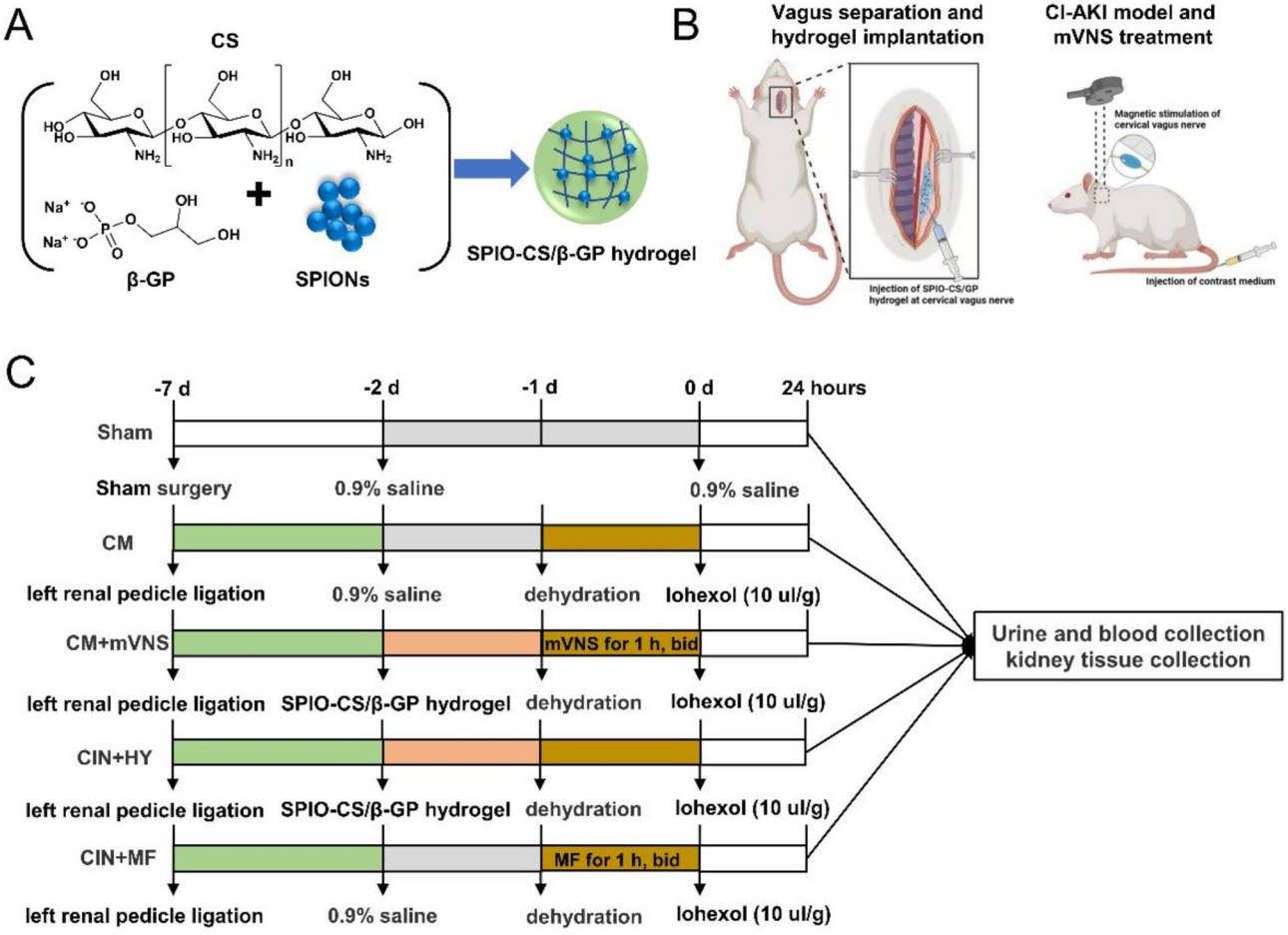

Fig. 1 Establishment of the magnetic stimulation system and experimental procedures. (**A**) The composition of the SPIO-CS/β-GP temperature-sensitive hydrogels. (**B**) SPIO-CS/β-GP hydrogel injection and magnetic vagus nerve stimulation. (**C**) Experimental procedures of mVNS treatment for CI-AKI. Sham group: Sham surgery without left renal pedicle ligation and 0.9% normal saline solution was injected instead of hydrogel; CM group: left renal pedicle ligation and iohexol injection; CM + mVNS group: additional SPIO-CS/β-GP hydrogel injection and magnetic stimulation; CM + hydrogel (CM + HY) group: additional SPIO-CS/β-GP hydrogel injection without magnetic stimulation; CM + magnetic field (CM + MF) group: magnetic stimulation without SPIO-CS/β-GP hydrogel injection

blotting and immunohistochemistry also indicated that mVNS can inhibit the expression of apoptosis-related proteins (Fig. 2E and F). However, CM + HY group and CM + MF group did not show the renoprotective effects, suggesting that the renoprotective role of mVNS requires systemic integrity.

Inhibition of exosome secretion by inhibitor GW4869 reversed the renoprotective effects of mVNS

To further study the role of plasma exosomes in the renoprotective effects of mVNS, we inhibited the release of exosomes by using the inhibitor GW4869. Figure 3A exhibited the schematic representation of experimental processing. As shown in Fig. 3B and C, GW4869 treatment reduced plasma exosome content after mVNS (Fig. 3B and C). Furthermore, we confirmed that GW4869 administration diminished the improvement in renal function, alleviation of pathological damage, and reduction in apoptosis brought about by mVNS treatment (Fig. 3D-F). These results suggest that circulating plasma exosomes following mVNS treatment are crucial in the mVNS-mediated improvement of CI-AKI.

Identification of circulating plasma exosomes and exosome tracking

With the aim to detect the characteristics of plasma exosomes, the blood samples of rats were collected immediately after the mVNS treatment. Both Sham-Exo and mVNS-Exo presented a round or oval membrane structure by using transmission electron microscope (TEM) (Fig. 4A). Nanoparticle tracking analysis (NTA) analysis exhibited that the sizes of Sham-Exo and mVNS-Exo mainly ranged from 80 to 200 nm (Fig. 4B). WB observed that proteins CD81, CD63, and TSG101 were positively expressed in both Sham-Exo and mVNS-Exo with no Calnexin expression (Fig. 4C). No significant difference

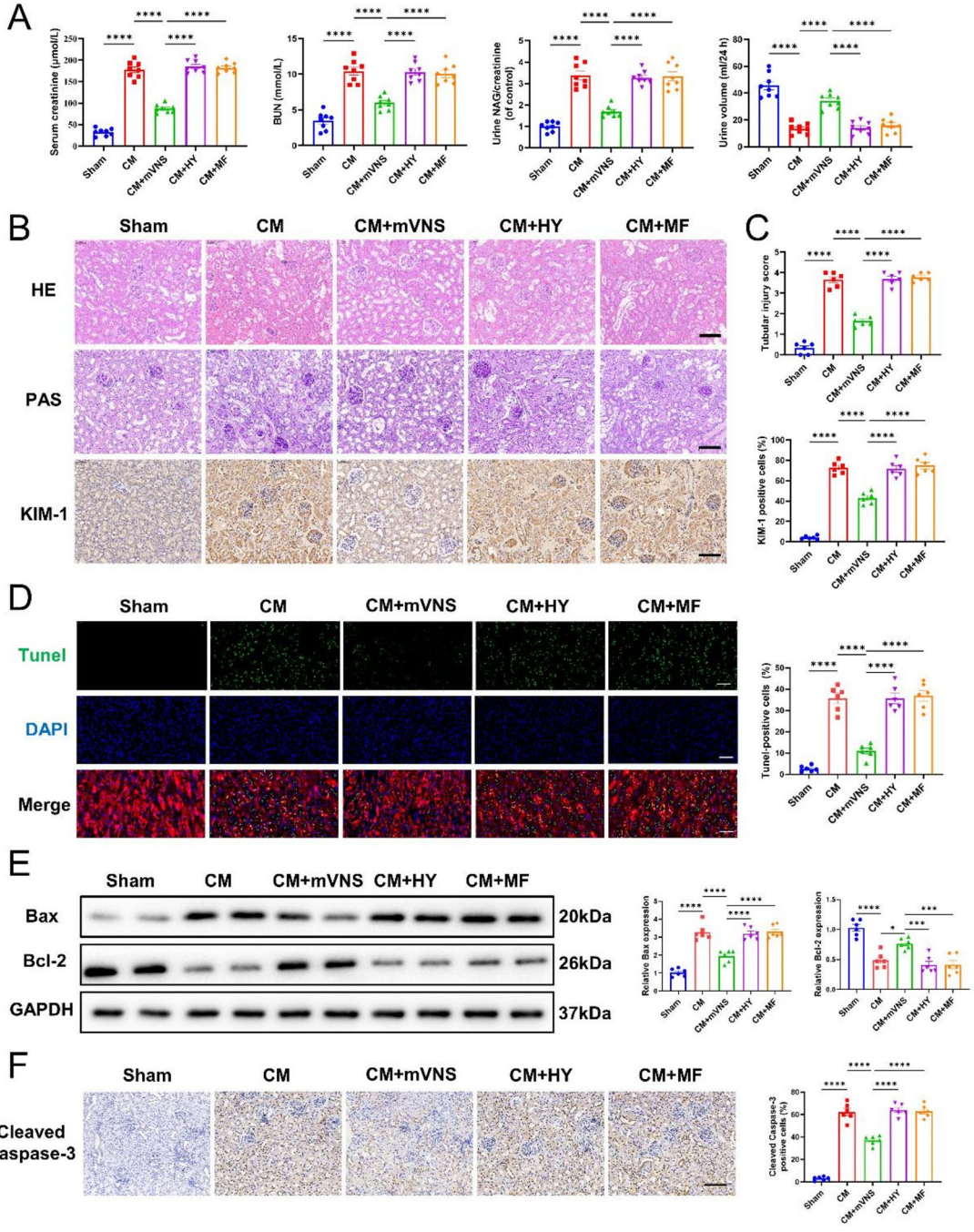

Fig. 2 mVNS treatment significantly attenuated iohexol-induced kidney injury and improved renal function. (**A**) Renal function was evaluated by detecting the content of SCr, BUN, NAG and 24 h urine volume, $n = 8$ per group. (**B**-**C**) Representative images of renal H&E, PAS and KIM-1 staining and quantitative analysis of renal tubular injury score and KIM-1 positive cells, $n = 6$ per group. Scale bar: 100 μm. (**D**) TUNEL analysis for effect of mVNS on apoptosis of renal tubular epithelial cells under CI-AKI. Green, TUNEL positive nuclei; Red, E-cadherin positive cell, considered as renal tubular epithelial cells; Blue, DAPI-stained nuclei, $n = 6$ per group. Scale bar: 50 μm. (**E**) Immunoblot analysis and quantification of Bax and Bcl-2 protein level in renal tissue, $n = 6$ per group, GAPDH as an internal control. (**F**) Representative images of renal cleaved caspase-3 staining and quantitative analysis of cleaved caspase-3 positive cells, $n = 6$ per group. Scale bar: 100 μm. Data are mean ± SEM. *indicates $p < 0.05$, ** indicates $p < 0.01$, *** indicates $p < 0.001$, and **** indicates $p < 0.0001$; All p values were obtained by one-way ANOVA

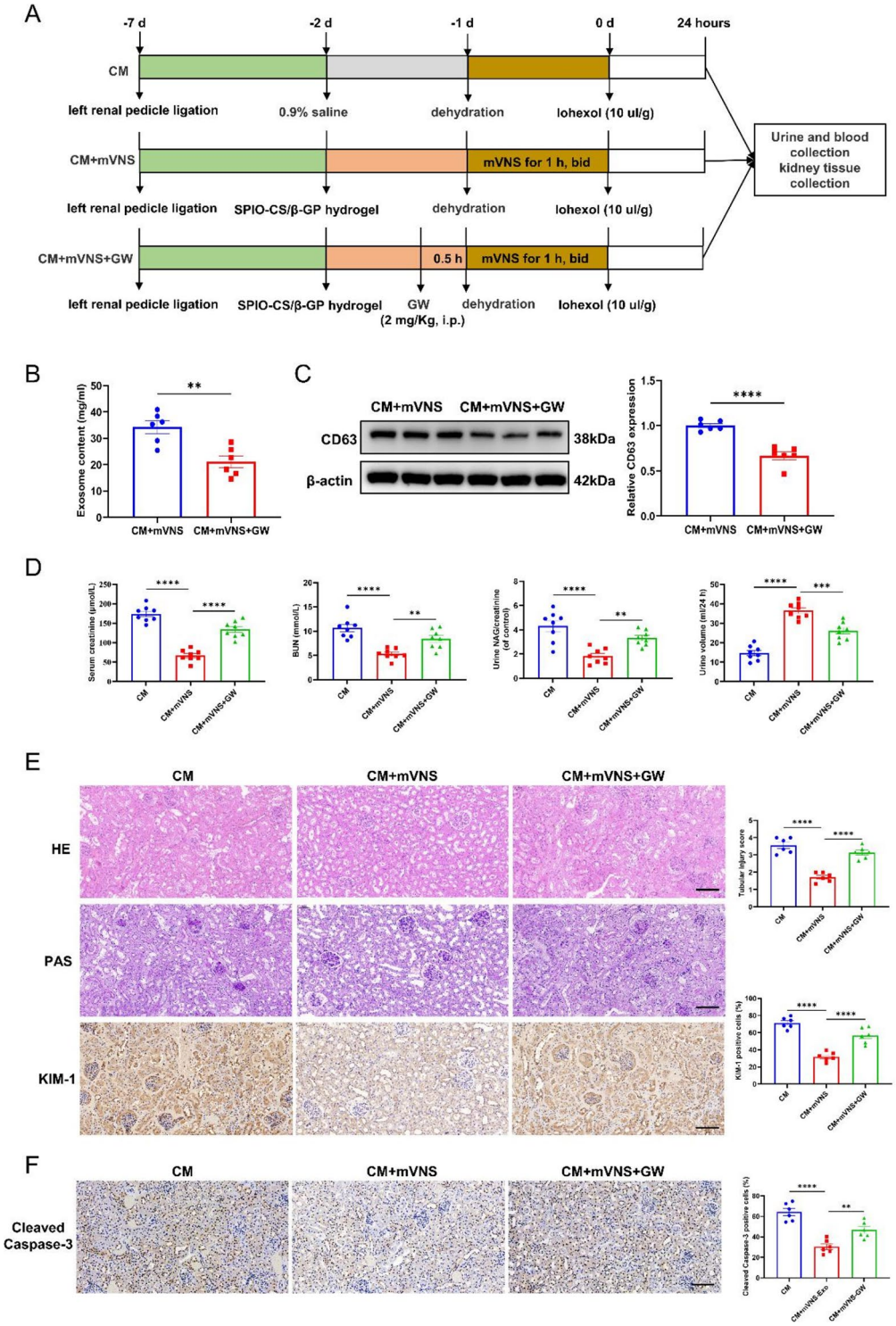

Fig. 3 Inhibition of exosome secretion by inhibitor GW4869 reversed the renoprotective effects of mVNS. (**A**) Schematic representation of experimental processing. (**B**) Quantitative analysis of Exosome content, $n = 6$ per group; (**C**) Western blot analysis of CD63 expression in exosomes, $n = 6$ per group. β-actin as an internal control. (**D**) Renal function was evaluated by detecting the content of SCr, BUN, NAG and 24 h urine volume, $n = 8$ per group. (**E**) Representative images of renal H&E, PAS and KIM-1 staining and quantitative analysis of renal tubular injury score and KIM-1 positive cells, $n = 6$ per group. Scale bar: 100 μm. (**F**) Representative images of renal cleaved caspase-3 staining and quantitative analysis of cleaved caspase-3 positive cells, $n = 6$ per group. Scale bar: 100 μm. Data are mean ± SEM. *indicates $p < 0.05$, ** indicates $p < 0.01$, *** indicates $p < 0.001$, and **** indicates $p < 0.0001$; All p values were obtained by one-way ANOVA or Student's t-test

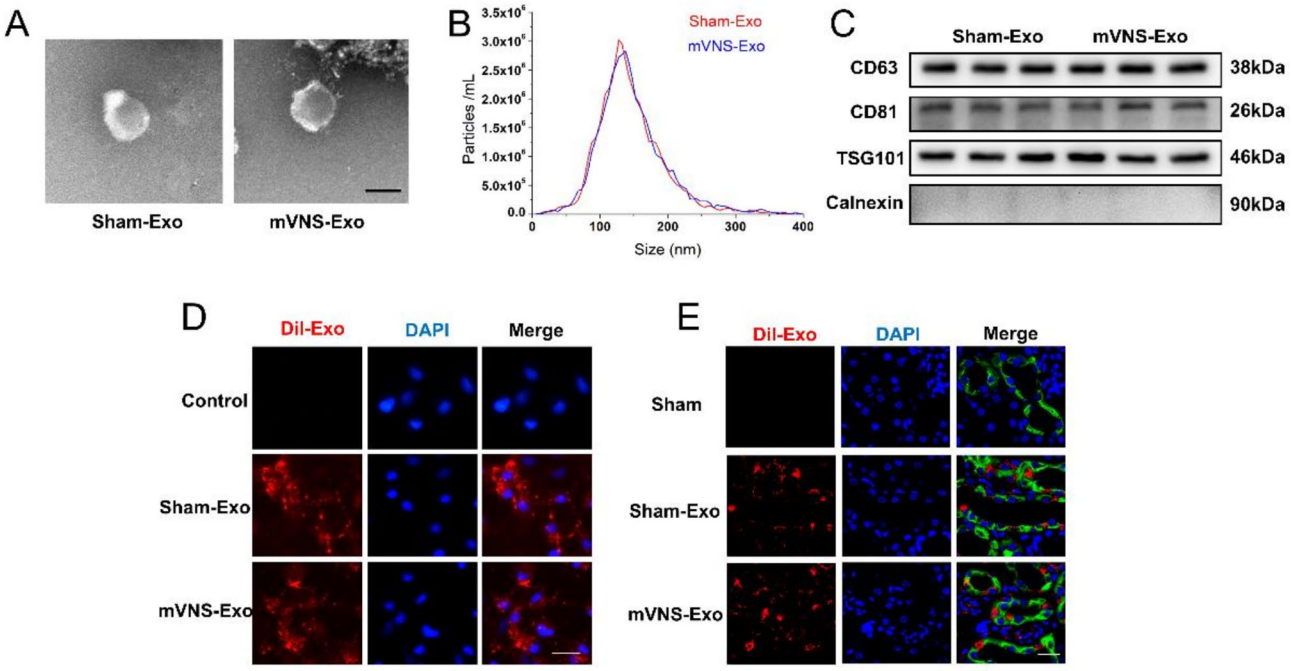

Fig. 4 Identification of circulating plasma exosomes and exosome tracking. (**A**) The morphology of circulating plasma exosomes was observed using TEM. Scale bar: 100 nm. (**B**) NTA was performed to detect the size distribution of Sham-Exo and mVNS-Exo. (**C**) Western blot showing the protein level of TSG101, CD63, CD81 and calnexin in Sham-Exo and mVNS-Exo, respectively. (**D**) NRK-52E were cultured in the presence or absence (Control) of DiI-labeled Sham-Exo or mVNS-Exo (red) for 24 h. The nucleus was stained with DAPI (blue). DiI-labeled exosomes were taken up by NRK-52E cells. Scale bars: 250 μm. (**E**) Rats were injected with 0.9% saline (Sham) or DiI-labeled Sham-Exo/mVNS-Exo through caudal vein and renal tissue was collected after 24 h. Representative images of triple immunostaining (red for DiR-labeled Exos, green for E-cadherin, considered as a marker for renal tubular epithelial cells, blue for DAPI). Scale bar: 20 μm

was observed in average size and marker protein expression between Sham-Exo and mVNS-Exo. Furthermore, after incubation with NRK-52E cells for 24 h, DiI-labeled Sham-Exo and mVNS-Exo were observed to migrate into the cytoplasm of NRK-52E cells (Fig. 4D). Similarly, intravenous injection of DiI-labeled exosomes into rats allowed for the observation of exosome uptake by renal tubular epithelial cells (Fig. 4F).

mVNS-Exo significantly attenuated iohexol-induced kidney injury and recovered renal functions

Compared to Sham-Exo, mVNS-Exo significantly improved iohexol-induced renal functional damage, as evidenced by a 55% reduction in Scr level, a 40% reduction in BUN level, a decreased NAG/creatinine ratio, and an increase in 24-hour urine output. (Fig. 5A). H&E and PAS staining suggested that mVNS-Exo could ameliorate pathological injuries in both renal glomeruli and tubules. Simultaneously, mVNS-Exo inhibited the expression of the KIM-1 molecule in renal tissues induced by iohexol (Fig. 5B and C). Furthermore, mVNS-Exo reduced the apoptosis in renal tubular cells and the expression of apoptosis-related proteins in renal tissues (Fig. 5D-F).

mVNS-Exo mitigated iohexol-induced injury in NRK-52E cells

Immunofluorescence showed that the iohexol-induced elevation of KIM-1 was markedly decreased by mVNS-Exo (Fig. 6A). In addition, TUNEL staining indicated that mVNS-Exo could protect NRK-52E cells from the apoptosis induced by iohexol. Consistently, iohexol significantly increased the expression of Bax and downregulated the expression of Bcl-2, while mVNS-Exo reversed their expressions induced by iohexol. However, Sham-Exo had no such protective effects (Fig. 6B and C). These results indicate that mVNS-Exo could inhibit iohexol-induced injury in NRK-52E cells.

The enrichment of mir-365-3p in mVNS-Exo is a crucial factor in ameliorating iohexol-induced injury in NRK-52E cells

This study revealed that mVNS treatment increased the renal levels of miR-365-3p, while treatments with CM, HY, and MF alone did not alter the expression levels of miR-365-3p (Fig. 7A). We extracted plasma exosomes under different treatments and found that miR-365-3p was significantly enriched in mVNS-Exo (Fig. 7B). We also conducted miRNA sequencing on Sham-Exo and mVNS-Exo, and selected miRNAs with a fold change

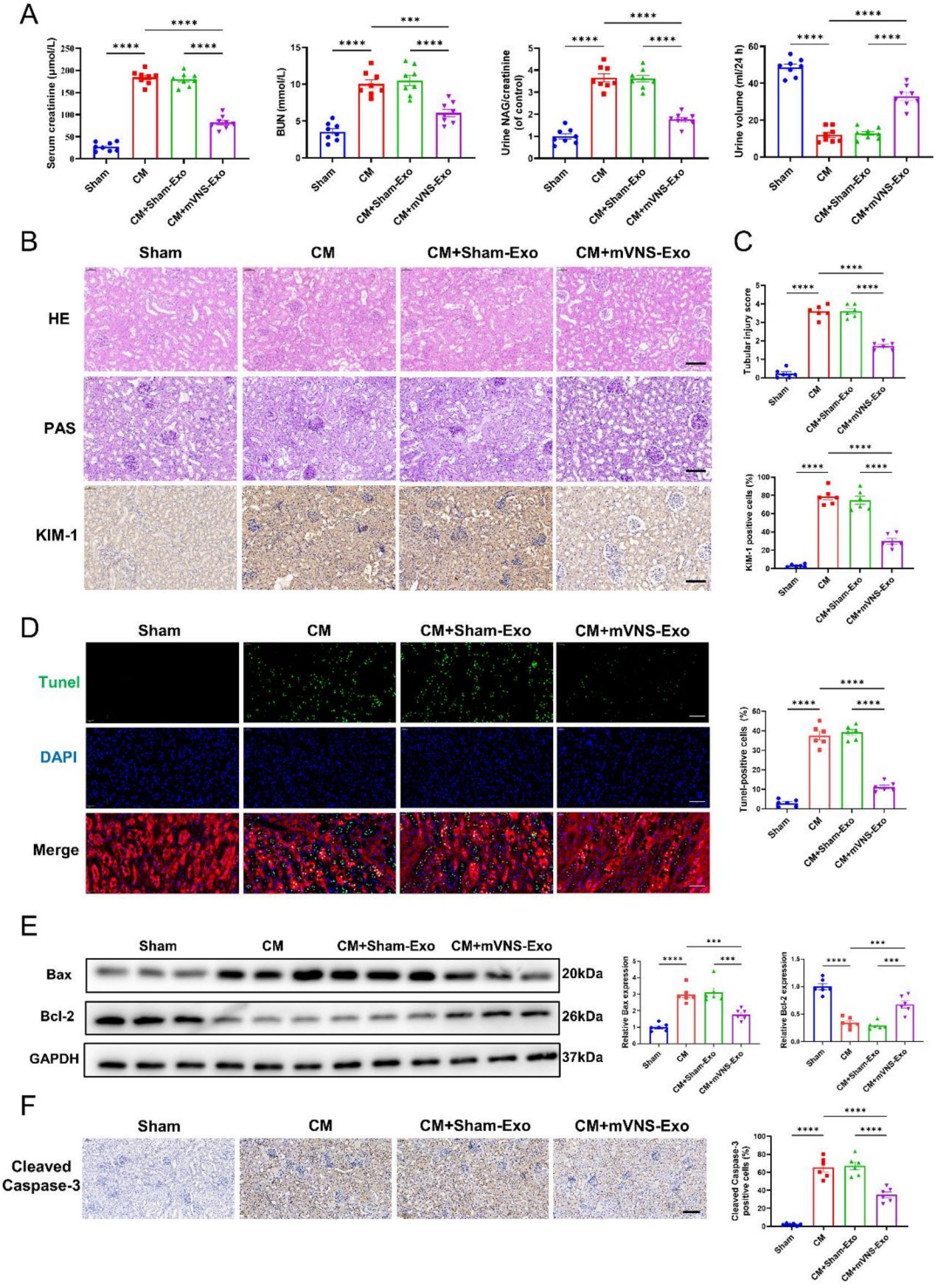

Fig. 5 mVNS-Exo significantly attenuated iohexol-induced kidney injury and improved renal function. (**A**) Renal function was evaluated by detecting the content of SCr, BUN, NAG and 24 h urine volume, $n = 8$ per group. (**B**-**C**) Representative images of renal H&E, PAS and KIM-1 staining and quantitative analysis of renal tubular injury score and KIM-1 positive cells, $n = 6$ per group. Scale bar: 100 μm. (**D**) TUNEL analysis for effect of mVNS on apoptosis of renal tubular epithelial cells under CI-AKI. Green, TUNEL positive nuclei; Red, E-cadherin positive cell, considered as renal tubular epithelial cells; Blue, DAPI-stained nuclei, $n = 6$ per group. Scale bar: 50 μm. (**E**) Immunoblot analysis and quantification of Bax and Bcl-2 protein level in renal tissue, $n = 6$ per group, GAPDH as an internal control. (**F**) Representative images of renal cleaved caspase-3 staining and quantitative analysis of cleaved caspase-3 positive cells, $n = 6$ per group. Scale bar: 100 μm. Data are mean ± SEM. *indicates $p < 0.05$, ** indicates $p < 0.01$, *** indicates $p < 0.001$, and **** indicates $p < 0.0001$; All p values were obtained by one-way ANOVA. Sham-Exo: derived from the plasma of rats underwent renal pedicle ligation before iohexol injection; mVNS-Exo: derived from the plasma of rats underwent renal pedicle ligation with mVNS pretreatment before iohexol injection

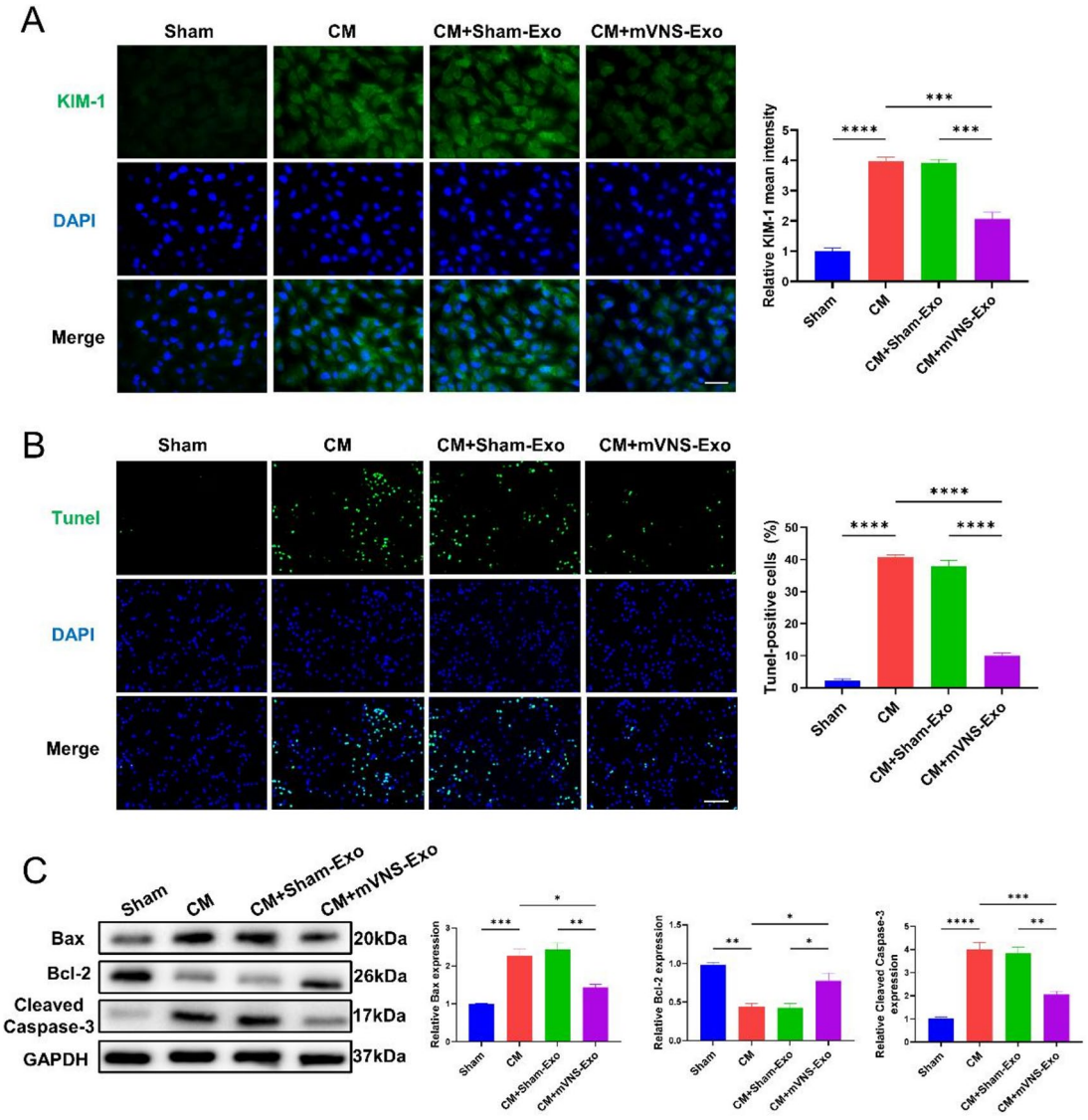

Fig. 6 mVNS-Exo mitigated iohexol-induced injury in NRK-52E cells. (**A**) Representative immunofluorescence staining of NRK-52E cells for KIM-1 (green) and DAPI (blue), and quantitative analysis of KIM-1 mean intensity, $n = 3$ per group. Scale bar: 200 μm. (**B**) TUNEL analysis for effect of Sham-Exo or mVNS-Exo on apoptosis of NRK-52E cells under CM. Green, TUNEL positive nuclei; Blue, DAPI-stained nuclei, $n = 3$ per group. Scale bar: 400 μm. (**C**) Immunoblot analysis and quantification of Bax, Bcl-2 and cleaved caspase-3 protein level in NRK-52E cells, $n = 3$ per group, GAPDH as an internal control. Data are mean ± SEM. *indicates $p < 0.05$, ** indicates $p < 0.01$, *** indicates $p < 0.001$, and **** indicates $p < 0.0001$; All p values were obtained by one-way ANOVA

greater than 3 times and higher abundance (miR-34b-5p, miR-365-3p, miR-29c-3p, miR-27a-3p, miR-374-5p) for PCR validation (Fig. S1A-B). The results showed that miR-365-3p was significantly highly expressed in mVNS-Exo compared to Sham-Exo (Fig. S1C). Furthermore, we demonstrated that mVNS-Exo treatment significantly increased the levels of miR-365-3p in vivo and in vitro (Fig. 7C and D). To explore whether the renoprotective effect of mVNS-Exo on CM mainly depended on miR-365-3p. NRK-52E cells were transfected with the miR-365-3p inhibitor, miR-365-3p mimics and mimics/inhibitor-NC, and then co-cultured with mVNS-Exo/Sham-Exo. Compared to the mVNS-Exo + inhibitor NC group, the miR-365-3p inhibitor reversed the effects of mVNS-Exo on reducing KIM-1 expression and decreasing apoptosis in NRK-52E cells. Similarly, compared to the Sham-Exo + mimics NC group, the addition of miR-365-3p mimics suppressed KIM-1 expression and reduced apoptosis in NRK-52E cells (Fig. 7E-G).

Mir-365-3p directly targeted Rheb and activated autophagy in NRK-52E cells

The results showed that, compared to the CM group, mVNS-Exo treatment exhibited elevated levels of autophagy, as evidenced by reduction of p62 expression, increase of LC3II/LC3I ratio and the presence of more autophagic

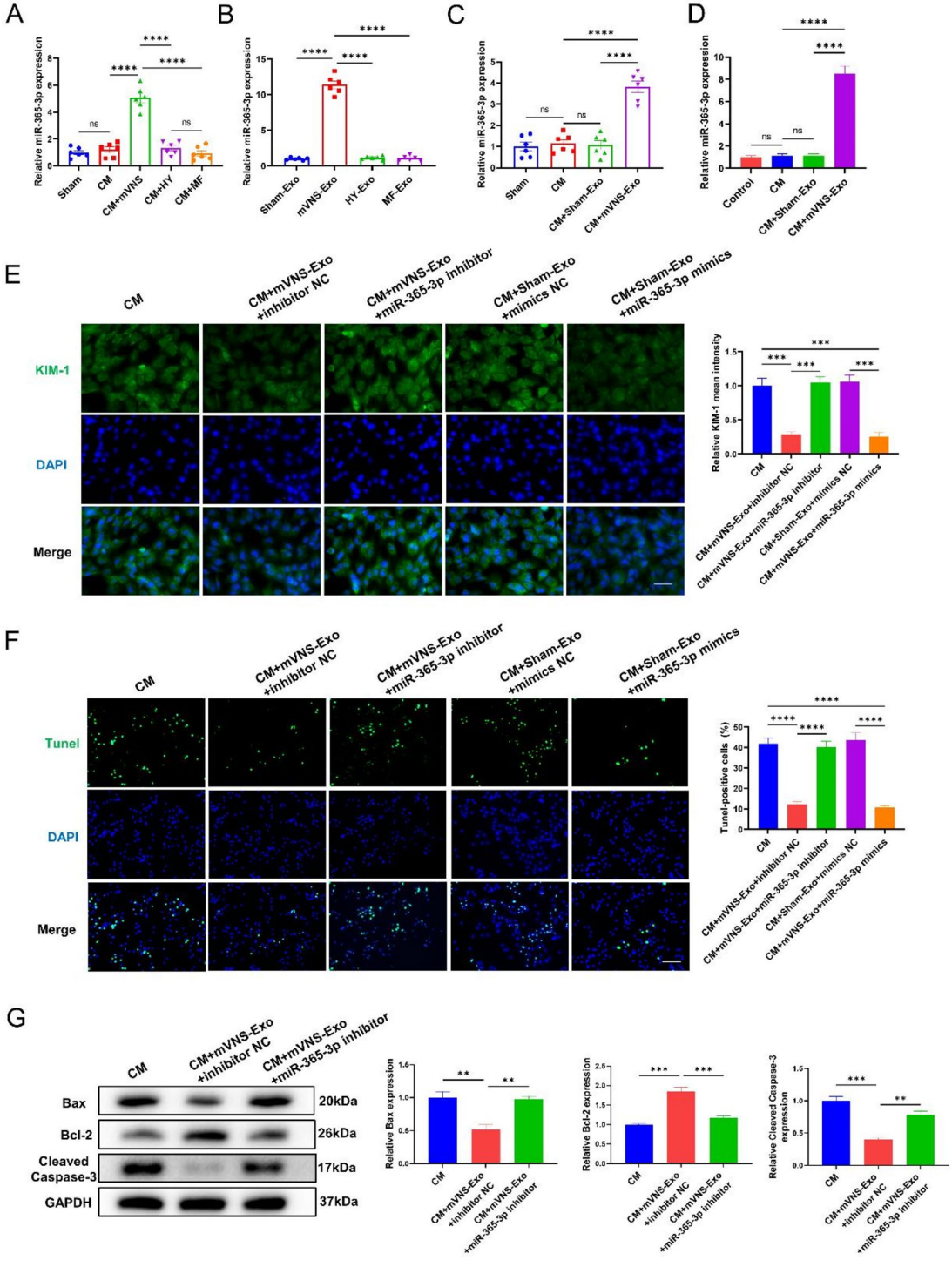

Fig. 7 The enrichment of miR-365-3p in mVNS-Exo is a crucial factor in ameliorating iohexol-induced injury in NRK-52E cells. (**A**) Quantitative real-time PCR analysis of miR-365-3p level in renal tissue. $n = 6$ per group. (**B**) Quantitative real-time PCR analysis of miR-365-3p level in exosomes. $n = 6$ per group. (**C**) Quantitative real-time PCR analysis of miR-365-3p level in renal tissue of rats injected with Sham-Exo or mVNS-Exo. $n = 6$ per group. (**D**) Quantitative real-time PCR analysis of miR-365-3p level in NRK-52E cells incubated with Sham-Exo or mVNS-Exo. $n = 3$ per group. (**E**) Representative immunofluorescence staining of NRK-52E cells for KIM-1 (green) and DAPI (blue), and quantitative analysis of KIM-1 mean intensity, $n = 3$ per group. Scale bar: 200 μm. (**F**) TUNEL analysis for effect of Sham-Exo or mVNS-Exo on apoptosis of NRK-52E cells under CM. Green, TUNEL positive nuclei; Blue, DAPI-stained nuclei, $n = 3$ per group. Scale bar: 400 μm. (**G**) Immunoblot analysis and quantification of Bax, Bcl-2 and cleaved caspase-3 protein level in NRK-52E cells, $n = 3$ per group, GAPDH as an internal control. Data are mean ± SEM. *indicates $p < 0.05$, ** indicates $p < 0.01$, *** indicates $p < 0.001$, and **** indicates $p < 0.0001$; All p values were obtained by one-way ANOVA

lysosomes under TEM. In contrast, Sham-Exo did not demonstrate any discernible effect on autophagy (Fig. 8A and B). Similarly, in NRK-52E cells, mVNS-Exo heightened the expression of LC3II/LC3I ratio and inhibited the expression of the P62 protein, while the miR-365-3p inhibitor counteracted the influence of mVNS-Exo on key autophagy proteins (Fig. 8C). Subsequently, we transfected NRK-52E cells with the mRFP-GFP-LC3 adenovirus, a commonly utilized autophagy marker. As shown in Fig. 8D, the number of autophagosomes (yellow spots) and autolysosomes (red spots) increased under mVNS-Exo treatment compared with the CM group. In parallel, miR-365-3p inhibitor suppressed the formation of autophagosomes and autolysosomes (Fig. 8D). Rheb, which is considered as a key protein in autophagy regulation, was identified as a potential target for miR-365-3p by TargetScan and miRDB (Fig. 9A). Luciferase reporter assays validated the interaction between miR-365-3p and Rheb as the luciferase activity of Rheb-wt in cells transfected with miR-365-3p was markedly suppressed along with the unaltered luciferase activity of Rheb-mut variant (Fig. 9B). Consistently, the protein levels of Rheb

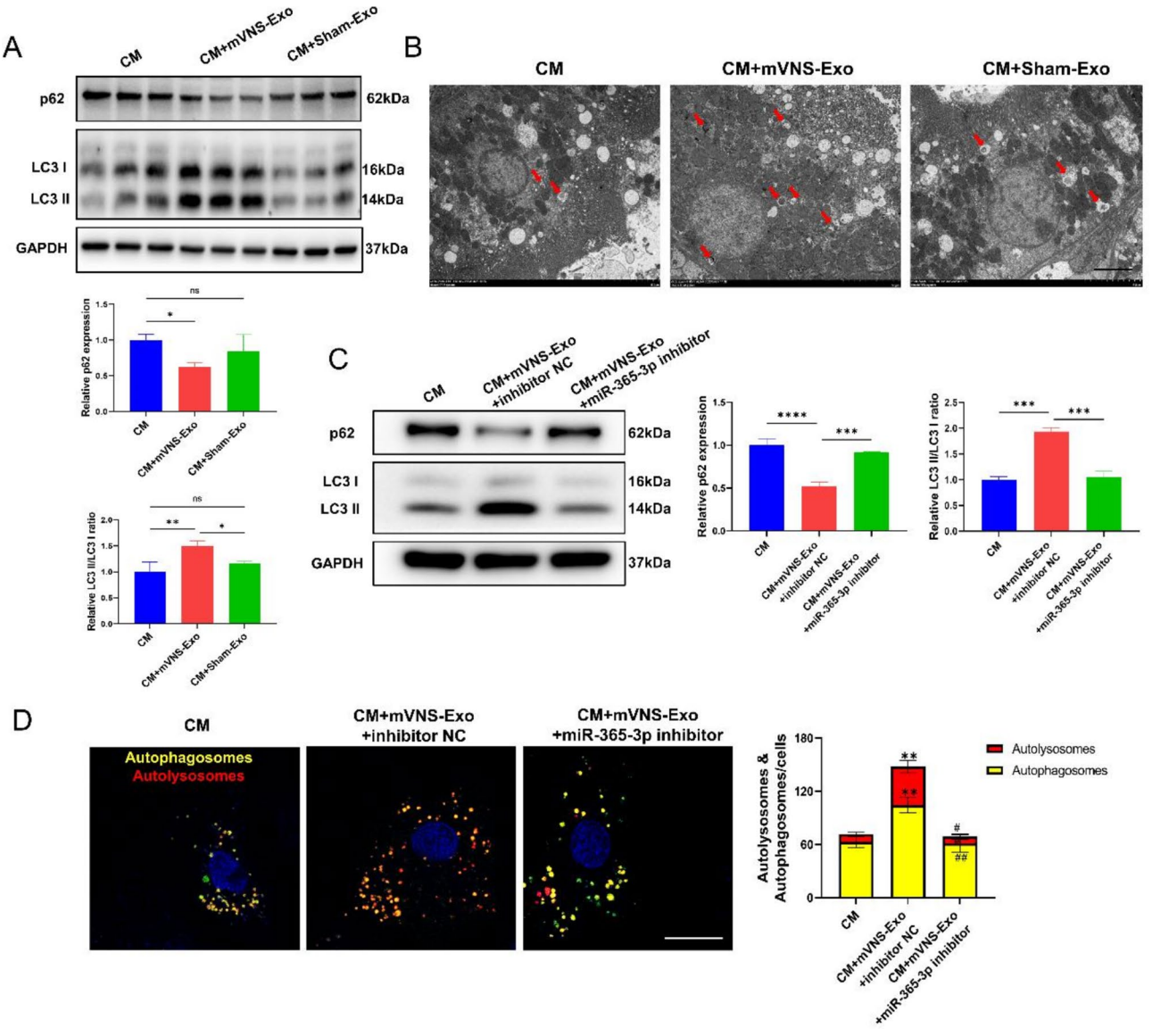

Fig. 8 mVNS-Exo enhanced the autophagy of NRK-52E cells under CM via miR-365-3p. (**A**) NRK-52E cells were treated with mVNS-Exo or mVNS-Exo. Immunoblot analysis and quantification of p62 protein level, LC3II/LC3I ratio in NRK-52E cells, $n=3$ per group, GAPDH as an internal control. (**B**) The morphology of autophagosomes was observed by TEM. The red arrow indicates the autophagosomes. Scale bar: 5 μm. (**C**) NRK-52E cells were treated with mVNS-Exo or mVNS-Exo + miR-365-3p inhibitor. Immunoblot analysis and quantification of p62 protein level, LC3II/LC3I ratio in NRK-52E cells, $n=3$ per group, GAPDH as an internal control. (**D**) Representative images and semi-quantitative analysis of autophagosomes (yellow dots in the merged image) and autolysosomes (red dots in the merged image) in NRK-52E cells, $n=3$ per group. Scale bar: 15 μm. ** $p<0.01$ versus CM group; $^{\#\#}p<0.01$ versus CM + mVNS + miR-365-3p inhibitor group

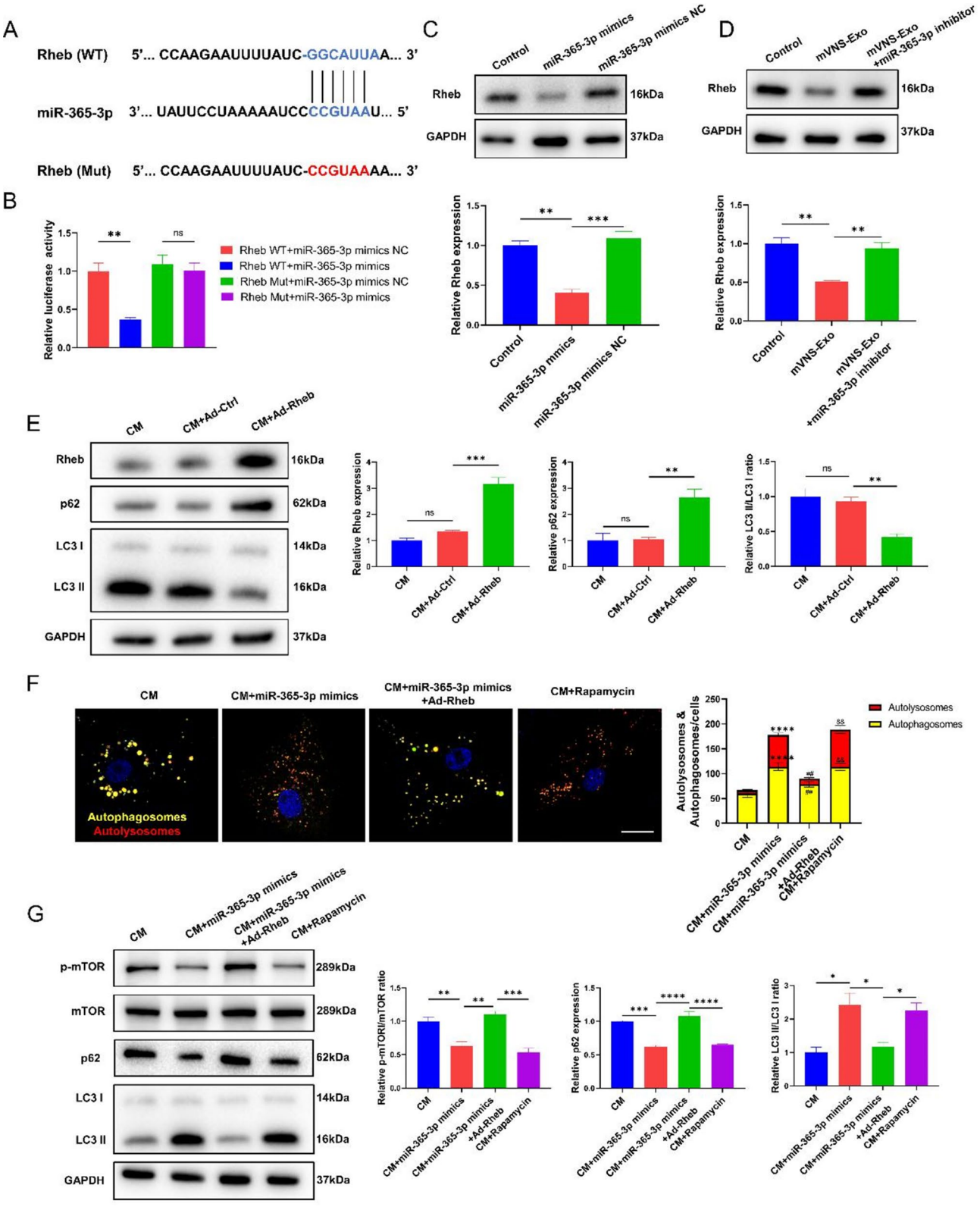

Fig. 9 (See legend on next page.)

(See figure on previous page.)

Fig. 9 miR-365-3p directly targeted Rheb in NRK-52E cells and overexpression of Rheb reversed the protective effect of miR-365-3p. (**A**) Predicted miR-365-3p target sequence in Rheb-3′ UTRs. Target sequences of Rheb-3′ UTRs were mutated. (**B**) Luciferase assay of 293T cells transfected with Rheb-3′ UTR-WT or Rheb-3′ UTR-Mut reporter together with mimics NC or miR-365-3p mimics ($n=3$). (**C**) Western blot analyzed Rheb protein levels in untreated NRK-52E cells (Control) and NRK-52E cells treated with mimics NC or miR-365-3p mimics, and quantification of Rheb protein level, $n=3$ per group, GAPDH as an internal control. (**D**) Western blot analyzed Rheb protein levels in NRK-52E cells treated with control (PBS), mVNS-Exo or mVNS-Exo + miR-365-3p inhibitor, and quantification of Rheb protein level, $n=3$ per group, GAPDH as an internal control. (**E**) NRK-52E cells were treated with Ad-Rheb or Ad-ctrl. Immunoblot analysis and quantification of p62 protein level, LC3II/LC3I ratio in NRK-52E cells, $n=3$ per group, GAPDH as an internal control. (**F**) Representative images and semi-quantitative analysis of autophagosomes (yellow dots in the merged image) and autolysosomes (red dots in the merged image) in NRK-52E cells, $n=3$ per group. Scale bar: 15 μm. $^{****}p<0.0001$ versus CM group; $^{\#\#}p<0.01$ versus CM + miR-365-3p mimics group. $^{\&\&}p<0.01$ versus CM + miR-365-3p mimics + Ad-Rheb group. (**G**) NRK-52E cells were treated with miR-365-3p mimics, miR-365-3p mimics + Ad-Rheb or Rapamycin. Immunoblot analysis and quantification of p62 protein level, LC3II/LC3I ratio and p-mTOR/mTOR ratio in NRK-52E cells, $n=3$ per group, GAPDH as an internal control. Data are mean ± SEM. *indicates $p<0.05$, ** indicates $p<0.01$, *** indicates $p<0.001$, and **** indicates $p<0.0001$; NS means not significant between groups. All p values were obtained by one-way ANOVA

were found to significantly decrease after the treatment of miR-365-3p mimics (Fig. 9C). After co-incubating with mVNS-Exo, we found that the expression of Rheb decreased in NRK-52E cells, while miR-365-3p inhibitor nullified the impact of mVNS-Exo in reducing Rheb expression (Fig. 9D). Therefore, there is a negative regulatory association between miR-365-3p and Rheb. Subsequently, Rheb was overexpressed to determine its effect on autophagy in NRK-52E cells under CM conditions. Western blot results showed the overexpression of Rheb in NRK-52E cells after the Adenoviruses-Rheb transfection. Compared to the CM group, overexpression of Rheb resulted in an elevated expression level of p62, a decreased LC3II/LC3I ratio, and inhibited autophagy levels in NRK-52E cells (Fig. 9E). Furthermore, while rapamycin was employed as a positive control, we validated that the capacity of miR-365-3p to inhibit mTOR phosphorylation and consequently promote autophagy in NRK-52E cells under CM exposure was abrogated by Rheb overexpression (Fig. 9F and G).

Discussion

The findings presented in this article provided the first evidence of the feasibility of mVNS for the treatment of CI-AKI. Through the injection of SPIO-CS/β-GP hydrogel to the left cervical vagal of SD rats followed by external magnetic field stimulation, we precisely enhanced vagus nerve activities and significantly reduced CI-AKI. We further proved that the nephroprotective effects of mVNS in vivo and in vitro were closely related to the plasma exosomes, where miR-365-3p was identified as the key exosomal miRNA responsible for inhibiting CM-induced apoptosis. Specifically, mVNS treatment elevated the miR-365-3p levels in plasma exosomes which were absorbed into the renal tubular epithelial cells, where miR-365-3p reduced the expression of its target gene Rheb and activated autophagy, thereby alleviating the apoptotic response induced by CM.

With the widespread use of CM, CI-AKI has emerged as a prevalent kidney injury disease and is now recognized as the third most common cause of renal insufficiency in hospitalized patients. This condition is linked to significant adverse clinical outcomes and poses a risk of mortality [45]. As there are currently no curative treatments for CI-AKI, the current optimal management strategy focuses on prevention. This includes the measures such as minimizing contrast media dosage and promoting fluid hydration [4, 46]. But there is no consensus on the optimal hydration regimen and it even has several drawbacks, such as the increment in likelihood of CI-AKI and death in patients [13]. Since electrical vagus nerve stimulation (eVNS) has been demonstrated to alleviate the AKI associated with IRI through by inhibiting inflammation, oxidative stress and apoptosis [18, 47], it prompts us to explore whether VNS can improve contrast-induced nephropathy. However, the limitations of eVNS have begun to emerge along with the researches progressing, including the adverse effects of the stimulation phase, complications of implantation surgery and problems regarding the devices implanted [23, 48–50]. In our previous research, we innovatively developed a new vagal modulation technique, the mVNS system. Unlike previous studies that relied solely on magnetic field stimulation of the vagus nerve, resulting in limited precision [51], our mVNS system involves the implantation of magnetic nanoparticles directly onto the target nerve. With external magnetic field stimulation, this system can precisely stimulate the vagus nerve, and have achieved promising results in the treatment of myocardial infarction and reperfusion injury [25, 26]. Motivated by these findings, we applied our mVNS system to rats receiving CM and observed a significant alleviation of impaired renal functions. This was evidenced by the reversal of elevated serum Cr, BUN, and urine NAG levels, as well as the restoration of diminished urine output. Moreover, mVNS treatment alleviated the damage to the renal tissue structure caused by CM, and suppressed KIM-1 expression and apoptosis in renal tubular epithelial cells.

In this study, we demonstrated for the first time the renoprotection of mVNS on CI-AKI. Previous studies indicated that the renal protective effect of VNS was mediated through the cholinergic anti-inflammatory pathway, which regulated the functions of immune cells and their production of pro-inflammatory cytokines to

suppress the inflammatory responses [52, 53]. A recent study illustrating the functional connections between VNS and exosomes has prompted us to investigate whether a similar association exists between mVNS and plasma exosomes [27]. In this article we confirmed that the application of exosomes from the plasma of rats undergoing mVNS significantly attenuated the kidney injuries and apoptosis in vitro and in vivo. Furthermore, we utilized the exosome inhibitor GW4869 to suppress exosome secretion in vivo. This intervention led to a reduction in the concentration of plasma exosomes under mVNS and weakened the protective effect of mVNS on CI-AKI, suggesting that the nephroprotective effects of mVNS were related to the plasma exosomes.

Plasma exosomes, released into the blood by the host cells of varied sources, facilitate remote communication by delivering cargos such as noncoding RNAs and proteins to the target cells and thus play vital roles in multiple diseases [54, 55]. Large bodies of studies have proposed the miRNAs present in plasma exosomes as the crucial molecules responsible for regulating remote organ functions [56–59]. In our study, we found the upregulated miR-365-3p expression in the plasma exosomes extracted from the rats undergoing mVNS. Additionally, in vitro experiments confirmed that circulating exosomal miR-365-3p can be absorbed by the renal tubular epithelial cells. Furthermore, miR-365-3p overexpression was shown to protect the kidneys against CI-AKI by regulating apoptosis and autophagy in renal tubular epithelial cells. In the classical CAP, vagus nerve stimulation can influence macrophages to regulate their functionality. Considering previous research indicating the enrichment of miR-365 in exosomes derived from macrophages [38, 60], it suggests that, following mVNS treatment, the plasma exosomes with elevated miR-365 expression may originate from macrophages. This warrants further investigation in our future work.

Autophagy is an intracellular pathway responsible for the targeted lysosomal degradation of damaged organelles, cellular macromolecules, and protein aggregates [43]. Recent studies reported that CM exposure partially activated cellular autophagy, which could be considered as a part of the compensatory mechanism to attenuate the tubular epithelial injuries [43, 61]. In detail, activation of autophagy significantly attenuated apoptosis to alleviate CI-AKI, while inhibition of autophagy can exacerbate CI-AKI [61–63]. In line with previous research findings, mVNS treatment resulted in the significant increase in LC3II/I ratio along with the reduced P62 expression, accompanied by a decrease in apoptosis under CM stimulation. These findings emphasized the crucial roles of mVNS in enhancing autophagy to mitigate CI-AKI. Functional studies proved the crucial roles of miR-365-3p in vitro in alleviating CM-induced apoptosis and regulating autophagy. Rheb, a small guanine triphosphate enzyme, belongs to the guanosine-binding protein Ras superfamily and plays important roles in apoptosis and autophagy [64–66]. Using online tools TargetScan and miRDB, we identified Rheb as the predicted target of miR-365-3p, which was later proved by luciferase reporter assays. We observed that overexpressed miR-365-3p significantly reduced Rheb expression, while overexpression of Rheb counteracted the pro-autophagic effect of miR-365-3p in NRK-52E cells. Therefore, we believe that mVNS could improve renal damage by regulating pathological molecular mechanisms compared to traditional hydration therapy. Moreover, the various regulatory effects of VNS on mitochondrial dysfunction, oxidative stress, and inflammation have been well established [67–69].

VNS has been used to treat various diseases in the clinic [70]. However, it is noteworthy that in some clinical trials, VNS therapy did not improve primary clinical outcomes [71, 72]. To address potential challenges that mVNS may face in clinical research, several strategies can be implemented. First, conducting large-scale, multicenter clinical trials, including diverse patient populations, encompassing different ages, ethnicities and comorbidities, would help validate its efficacy across various groups. Second, incorporating long-term follow-up could assess the durability of treatment effects and safety profiles. Additionally, real-world evidence from observational studies could complement clinical trial data.

This study has the following limitations. Firstly, although we employed the stimulation parameters derived from our previous study and successfully achieved the significant improvement of CM-damaged renal functions, we still need to develop and establish the personalized protocols regarding the optimal stimulation parameters for the maximum therapeutic effects. Secondly, considering the diverse sources of exosomes in circulation, it would be highly valuable in future studies to identify the primary sources of releasing plasma exosomes with nephroprotective effects induced by mVNS. Such identification could significantly enhance the clinical applicability of our findings.

In summary, we herein firstly applied the mVNS system to prevent CI-AKI. We further demonstrated that the elevated miR-365-3p in circulating plasma exosomes from the rats undergoing mVNS played a pivotal role in improving CI-AKI. miR-365-3p significantly enhanced autophagy and reversed CM-induced apoptosis in renal tubular epithelial cells through inhibiting the expression of its target gene Rheb. As a result, our findings highlight the promising therapeutic potential of mVNS on CI-AKI, suggesting that mVNS is expected to be an important supplement in the treatment of CI-AKI in clinical practice.

Methods

Animal preparation and establishment of the CI-AKI model

Sprague-Dawley (SD) rats (male, about 220 g) were purchased from Beijing Vital River Laboratory Animal Technology Company and the conducted in accordance with the Guide for the Care and Use of Laboratory Animals published by the US National Institutes of Health. The CI-AKI model in rats was established based on a previously published protocol [73]. All the rats were anesthetized by intraperitoneal injection of 1% pentobarbital sodium (40 mg/kg). The left renal pedicle of rats was first ligated to abolish the left renal function. At one week after the operation, the rats were dehydration for 24 h and then were injected iohexol (10 μl/g, GE healthcare, the United States) via the tail vein. After 24 h, the rats were sacrificed to extract the urine, blood and kidney tissues for the following analysis.

Isolation and characterization of plasma exosomes

Sham-Exo is derived from the plasma of rats underwent renal pedicle ligation before iohexol injection, while mVNS-Exo is derived from the plasma of rats underwent renal pedicle ligation with mVNS pretreatment before iohexol injection. Plasma exosomes were isolated using a sequential differential centrifugation method [74]. The plasma samples were initially centrifuged at 500×g for 30 min and then at 2000×g for 30 min to eliminate blood cells and cellular debris. The resulting supernatants underwent centrifugation at 110,000×g for 120 min, yielding plasma exosomes as the final pellets at the tube bottom. All procedures were conducted at 4 °C. The isolated exosomes were resuspended in PBS and stored at -80 °C. The protein concentrations of exosomes were determined using the BCA protein assay. Subsequently, the surface markers of exosomes were detected by western blotting using antibodies against TSG101, CD63, and CD81 (Santa Cruz, USA). The morphology and structure of exosomes were identified through transmission electron microscopy (TEM, FEI-Tecnai G2), while the size distribution and concentration of exosomes were assessed using nanoparticle tracking analysis (NTA) with ZetaView PMX 110.

Establishment of the mVNS system and experimental groups

The mVNS system included the SPIO-CS/β-GP hydrogel and an external magnetic field (100mT, 20 Hz) to send pulse sequences. Two days before injecting iohexol, 0.2 ml volume SPIO-CS/β-GP hydrogel synthesized as previously described [25] were injected around the left vagus nerve using a syringe, and the hydrogel solidified and completely wrapped the nerve after 5 min. The rats were divided into 5 groups (n=8): (1) Sham group: Sham surgery without left renal pedicle ligation and 0.9% normal saline solution was injected instead of hydrogel; (2) CM group: left renal pedicle ligation and iohexol injection; (3) CM+mVNS group: additional SPIO-CS/β-GP hydrogel injection and magnetic stimulation; (4) CM+hydrogel (CM+HY) group: additional SPIO-CS/β-GP hydrogel injection without magnetic stimulation; (5) CM+magnetic field (CM+MF) group: magnetic stimulation without SPIO-CS/β-GP hydrogel injection. Intraperitoneal injection of GW4869 at the dose of 2 mg/kg was chosen based on previous studies [75, 76]. To study whether the recovery of renal functions was related to the plasma exosomes after mVNS, the rats were divided into 4 groups (n=8): (1) Sham group; (2) CM group; (3) CM+Sham-Exo: additional intravenously injecting Sham-Exo (2.5 mg/kg) before iohexol injection; (4) CM+mVNS-Exo: additional intravenously injecting mVNS-Exo (2.5 mg/kg) before iohexol injection.

Collection of urine, blood and kidney samples

Rats in each group were raised in the metabolic cages to collect urine for 24 h and detect the urine volume and N-acetyl-β-D-glucosaminidase in the urine. After being anesthetized by pentobarbital, the blood samples were collected from the tail tips and centrifuged at 3,000×g for 15 min to get the serum for the detection of BUN and SCR by ELISA assay. The right kidney tissues were collected immediately from each rat at the end of the experiment, which were then coronally dissected. Half of the kidney was fixed with 4% paraformaldehyde for histological examination, while the left half was frozen in liquid nitrogen for the following extraction of RNA and proteins.

Histology and immunohistochemistry (IHC) staining

Both hematoxylin-eosin (H&E) staining and periodic acid-Schiff (PAS) staining were used to evaluate the histological changes of the kidney. After being fixed in 4% paraformaldehyde, dehydrated, and embedded in paraffin, the kidney tissues were sectioned at a thickness of 4 μm and then stained with hematoxylin-eosin (C0105S, Beyotime, China) or Periodic acid–Schiff solutions (BA4114, Baso, China) for detecting the histopathological changes of kidney tissues. Renal tubule injuries were assessed by evaluating the degree of loss of the brush borders, foaming and the detachment of renal tubular cells. Scores were assigned on the following scale: no injury (0); mild: 0-25% (1); moderate: 25-50% (2); severe: 51-75% (3); and very severe: 76-100% (4) [77]. For immunohistochemical staining, the kidney sections were incubated with antibodies against KIM-1 (10 μg/ml, NBP1-76701, Novus, USA) or Cleaved-Caspase-3 (1:1000, 9664, CST, USA) overnight at 4℃. Then the sections were incubated with secondary antibodies (1:5000, FDR007, FUDE Bio, China) and then DAB kit to visualize the antigen

(ZLI-9018, Beijing, China). The sections were observed with under a light microscope (TE2000-U, Nikon, Japan) and were analysed using Image-Pro Plus 6.0.

ELISA assay

The NAG in urine and BUN and Scr in blood were detected by using ELISA kits according to the manufacturer's instructions. ELISA kits included NAG (CSB-E07443r, CUSABIO, China), BUN (HM-E20555R1, HUAYUN, China) and Scr (RX301570R, HUAYUN, China).

Cell culture, iohexol exposure and transfections

Rat renal tubule epithelial cells (NRK-52E) were purchased from Shanghai Cell Bank (Shanghai, China) and were cultured in DMEM/F12 containing 10% fetal bovine serum (FBS) (10099141 C, Gibco, USA) and 1% penicillin/streptomycin (15070063, Gibco, USA Gibco) in 5% CO_2 at 37 °C. When growing to about 80% confluence, the cells were treated as follows. To evaluate the effects of mVNS-Exo on CM-induced injuries, NRK-52E cells were divided into 4 groups, as follows: (1) control group; (2) CM group; (3) CM + Sham-Exo group; (4) CM + mVNS-Exo group. In detail, NRK-52E cells in CM group were exposed to iohexol (20mgI/ml) for 72 h, while CM + Sham-Exo group and CM + mVNS-Exo group were incubated with iohexol (20mgI/ml) and Sham-Exo or mVNS-Exo (50 μg/mL) for 72 h. To confirm the modulation of miR-365-3p to Rheb expression, miR-365-3p mimics (100nM), miR-365-3p inhibitor (100nM) and negative control (100nM) synthesized by RiboBio (China) were transfected to NRK-52E cells via riboFECT™ CP Reagent (C10511-05, RiboBio, China) according to the manufacturer's instructions. Adenoviruses-Rheb (Ad-Rheb) was generated according to the manufacturer's protocol (Genechem Technology, China). NRK-52E cells were infected with Ad-Rheb at a multiplicity of infection of 50 for 24 h, as well as Ad-ctrl as a negative control. Western blot analysis was performed to determine the infection efficiency. To monitor autophagic flux, NRK-52E cells cells were transfected with mRFP-GFP-LC3 adenovirus (Hanbio, HB-AP210 0001, Shanghai, China) at a concentration of 10^10 PFU/mL for 48 h. The quantification of autophagic flux in NRK-52E cells was achieved by enumerating the yellow and red dots. Rapamycin (100 nM) were incubated with cells for 2 h before adding iohexol.

Exosomal miRNA sequencing

The miRNAs sequencing was carried out in Sham-Exo and mVNS-Exo. Exosomal miRNA-seq analysis was performed by Shanghai Bioprofile Technology Company Ltd. (Shanghai, China) using the Illumina NovaSeq Xplus. Diferentially expressed miRNAs were identifed through |log2(fold change)|≥1 and P-value < 0.05 with the threshold set for up and downregulated genes. Bioinformatics analyses, including differential expression analysis of miRNAs, prediction of miRNA target genes, gene ontology (GO) analysis, and Kyoto Encyclopedia of Genes and Genomes (KEGG) pathway enrichment analysis, were conducted by Shanghai Bioprofile Technology Company Ltd.

TUNEL staining

The TdT-mediated dUTP Nick-End Labeling (TUNEL) kit (11684795910, Roche Life Science, Switzerland) was applied to detect apoptosis in vivo and in vitro, according to the manufacturer's protocol. To detect the apoptosis in renal tissues, the dewaxed sections were permeabilized with 0.1 M sodium citrate for 30 min and then incubated with TUNEL reaction mixtures in the dark at 37℃ for 1 h. To detect the apoptosis in NRK-52E cells, after being washed with PBS and fixed for 20 min with 4% paraformaldehyde, the cell samples were stained with the TUNEL kit. E-cadherin was considered as a marker for renal tubular epithelial cells. Cells with TUNEL-positive nuclei and TUNEL-negative nuclei were counted in by using fluorescence microscopy (Axio Vert A1, Zeiss, Germany) and quantified by Image-Pro Plus 6.0.

Immunofluorescent staining

NRK-52E cells were washed with PBS (pH 7.4), fixed in 4% paraformaldehyde for 25 min and permeabilized with 0.2% Triton X-100 for 20 min at room temperature. After blocked in PBS containing 1% BSA, cells were incubated with the antibody against KIM-1 (20 μg/ml, NBP1-76701, Novus, USA) for overnight incubation at 4 °C. The cells washed with PBS three times for 5 min, then were incubated with secondary antibody for 2 h, while the nucleus was stained with 4′,6-diamidino-2-phenylindole (DAPI) (100 ng/ml) for 5 min at room temperature. The KIM-1 expression was evaluated by using fluorescence microscopy (Axio Vert A1, Zeiss, Germany).

Transmission electron microscope (TEM) analysis

TEM was applied to observe the formation of autophagosomes in kidney tissue. Briefly, kidney tissues with volume of less than 1 mm [3] were fixed in 2.5% glutaraldehyde for 2 h, followed by conventional dehydration, osmosis, embedding, sectioning, and staining as previously described [78].

Luciferase reporter assay

Luciferase reporters containing wild-type or mutant 3'UTR of Rheb (Rheb-WT or Rheb-MUT) were constructed by RiboBio (China). For the luciferase assay, HEK-293T cells growing to about 80% confluence in 24-well plates were transfected with 100 ng luciferase

reporters containing Rheb-WT or Rheb-MUT per well and 100nM miR-365-3p mimics or mimics-NC per well using riboFECT™ CP Reagent. Cells were harvested at 48 h after transfection and the luciferase activities were detected using the Dual Luciferase Reporter Assay Kit (11402ES60, YEASEN, China) according to the instructions. Firefly luciferase activities were normalized to Renilla luciferase activity.

Western blotting analysis

Western blotting analysis was performed according to the standard protocol as previously described [78, 79]. Antibodies used were as follows: Bax (1:1000, 14796, Cell Signaling Technology/CST, USA), Bcl2 (1:5000, ab196495, Abcam, UK), CD63 (1:500, sc-5275, Santa Cruz, USA), CD81(1:1000, sc-166029, Santa Cruz, USA), Cleaved-Caspase-3 (1:1000, 9664, CST, USA), GAPDH (1:10000, ab181602, Abcam, UK), LC3A/B (1:1000, 12741, CST, USA), mTOR (1:1000, 2797, CST, USA), phospho-mTOR(Ser-2448) (1:1000, 2796, CST, USA), P62 (1:1000, ab109012, Abcam, UK), Rheb (1:1000, ab25873, Abcam, UK) and TSG101 (1:500, sc-7964, Santa Cruz, USA). The bands were visualized by enhanced chemiluminescence reagents and analysed with a gel documentation system (Bio-Rad Gel Doc1000 and Multi-Analyst version 1.1).

Quantitative real-time polymerase chain reaction (qRT-PCR) analysis

Total RNAs from cells and tissues were extracted by Trizol (RC202-01, Vazyme, China) and the concentrations of RNAs were examined by a spectrophotometer (NanoDrop-2000, Thermo Scientific, USA). The isolated RNAs were then reverse-transcribed to cDNA with the Hifair III 1st Strand cDNA Synthesis SuperMix for qPCR (1141ES10, Yeasen, China). Quantitative PCR analysis was performed by Hieff qPCR SYBR Green Master Mix (11203ES08, Yeasen, China) and QuantStudio3 Real-Time PCR Systems (Thermo Scientific, USA) in accordance with the manufacturer's instructions. 18s ribosomal RNA (18s) was used the reference gene for the expression of Rheb gene. For RNAs in exosomes, the Total exosome RNA isolation kit (4478545, Thermo Scientific, USA) the was applied to extract exosomal RNAs, following the manufacturer's protocols. For quantification of miR-365-3p, cDNAs were synthesized with the miRNA First-Strand cDNA Synthesis Kit (by stem-loop) (MR101-02, Vazyme, China), which were examined by quantitative PCR analysis with AceQ qPCR SYBR Green Master Mix (Q111-03, Vazyme Biotech, China) and QuantStudio3 Real-Time PCR Systems (Thermo Scientific, USA). U6 was the reference gene for the expression of miR-365-3p in cells, while cel-miR-39 was used as the reference gene of miR-365-3p expression in exosomes.

Statistical analysis

Continuous variables are expressed as mean±SEM. Unpaired, two-tailed Student's t-test was used to compare continuous variables between the two groups. One way analysis of variance (ANOVA) with Bonferroni's or Tukey's correction was used for multi-group comparison. All statistical tests were performed using GraphPad Prism software version 8.0, and a 2-sided $p<0.05$ was considered statistically significant (*indicates $p<0.05$, ** indicates $p<0.01$, *** indicates $p<0.001$, and **** indicates $p<0.0001$). NS means not significant between groups.

Abbreviations

CI-AKI	Contrast-induced acute kidney injury
CM	Contrast media
VNS	Vagus nerve stimulation
mVNS	Magnetic vagus nerve stimulation
eVNS	Electrical vagus nerve stimulation
Scr	Serum creatinine
BUN	Blood urea nitrogen
NAG	Urinary N-acetyl-β-D-glucosaminidase
KIM-1	Kidney injury molecule-1
CS/β-GP	Chitosan-β-glycerophosphate
SPIO	Superparamagnetic iron oxide
Exo	Exosomes
Rheb	Ras homolog enriched in brain
CAP	Cholinergic anti-inflammatory pathway
NTA	Nanoparticle tracking analysis

Supplementary Information

The online version contains supplementary material available at https://doi.org/10.1186/s12951-024-02928-0.

Supplementary Material 1

Supplementary Material 2

Author contributions

T.Y.W., W.W.Z., and Y.L. designed and performed the experiments, analyzed data, and wrote the manuscript; R.D., K.Y.C., and S.Y.B. performed experiments and analyzed data; J.F.S., B.H., Y.Q.C., and Y.L. provided critical suggestions and technical support; All authors reviewed the manuscript.

Funding

This study was supported by the grants from National Natural Science Foundation of China (Grant No. 82300444 and 82370329), Science and Technology Talent Trusted Project of Jiangsu Province (JSTJ-2024-339), Traditional Chinese Medicine Science and Technology Development Plan of Jiangsu Province (QN202323) and the Youth Medical Science and Technology Innovation Project of Xuzhou Municipal Health Commission (XWKYHT20200067). We would like to acknowledge the financial support from National Natural Science Foundation of China (Grant No. 82200449).

Data availability

The datasets generated or analysed in this study can be obtained upon reasonable request from the corresponding author.

Declarations

Ethics approval and consent to participate

All animal study protocols were approved by the Ethics Committee of Xuzhou Medical University and conducted in accordance with the Guide for the Care and Use of Laboratory Animals.

Competing interests

The authors declare no competing interests.

Author details
[1]XuZhou Clinical School of Xuzhou Medical University, Department of Central Laboratory, Xuzhou Central Hospital, No.199 Jiefang South Road, Xuzhou 221009, P.R. China
[2]XuZhou Clinical School of Xuzhou Medical University, Department of Cardiology, Xuzhou Central Hospital, XuZhou Institute of Cardiovascular disease, No.199 Jiefang South Road, Xuzhou 221009, P.R. China
[3]The State Key Laboratory of Bioelectronics, Jiangsu Key Laboratory of Biomaterials and Devices, School of Biological Science and Medical Engineering, Southeast University, Nanjing 210009, P.R. China
[4]Section of Pacing and Electrophysiology, Division of Cardiology, The First Affiliated Hospital of Nanjing Medical University, Guangzhou Road 300, Nanjing 210029, P.R. China
[5]Department of Cardiology, The Affiliated Suzhou Hospital of Nanjing Medical University, Suzhou Municipal Hospital, Gusu School, Nanjing Medical University, Suzhou 215000, PR China

Received: 10 February 2024 / Accepted: 10 October 2024
Published online: 28 October 2024

References

1. Palli E, Makris D, Papanikolaou J, et al. Contrast-induced nephropathy in aged critically ill patients. Oxid Med Cell Longev. 2014;2014:756469.
2. Amin AP, Bach RG, Caruso ML, et al. Association of Variation in contrast volume with acute kidney Injury in patients undergoing percutaneous coronary intervention. JAMA Cardiol. 2017;2(9):1007–12.
3. Valle JA, McCoy LA, Maddox TM et al. Longitudinal risk of adverse events in patients with acute kidney Injury after Percutaneous Coronary intervention: insights from the National Cardiovascular Data Registry. Circ Cardiovasc Interv. 2017;10(4).
4. Almendarez M, Gurm HS, Mariani J Jr., et al. Procedural strategies to reduce the incidence of contrast-Induced Acute kidney Injury during Percutaneous Coronary intervention. JACC Cardiovasc Interv. 2019;12(19):1877–88.
5. Kusirisin P, Chattipakorn SC, Chattipakorn N. Contrast-induced nephropathy and oxidative stress: mechanistic insights for better interventional approaches. J Translational Med. 2020;18(1):400.
6. Lin Q, Li S, Jiang N, et al. PINK1-parkin pathway of mitophagy protects against contrast-induced acute kidney injury via decreasing mitochondrial ROS and NLRP3 inflammasome activation. Redox Biol. 2019;26:101254.
7. Solomon R, Dauerman HL. Contrast-induced acute kidney injury. Circulation. 2010;122(23):2451–5.
8. Ludes PO, de Roquetaillade C, Chousterman BG, et al. Role of damage-Associated molecular patterns in septic acute kidney Injury, from Injury to Recovery. Front Immunol. 2021;12:606622.
9. Maaniitty T, Stenstrom I, Uusitalo V, et al. Incidence of persistent renal dysfunction after contrast enhanced coronary CT angiography in patients with suspected coronary artery disease. Int J Cardiovasc Imaging. 2016;32(10):1567–75.
10. Cheng AS, Li X. The potential biotherapeutic targets of contrast-Induced Acute kidney Injury. Int J Mol Sci. 2023;24(9).
11. Maksimczuk J, Galas A, Krzesinski P. What promotes acute kidney Injury in patients with myocardial infarction and multivessel coronary artery disease-contrast media, hydration status or something. Else? Nutrients. 2022;15(1).
12. Wang Z, Song Y. Role of hydration in contrast-Induced Nephropathy in patients who underwent primary percutaneous coronary intervention. Int Heart J. 2019;60(5):1077–82.
13. Liu Y, Li H, Chen S et al. Excessively high hydration volume may not be Associated with decreased risk of contrast-Induced Acute kidney Injury after Percutaneous Coronary intervention in patients with renal insufficiency. J Am Heart Assoc. 2016;5(6).
14. Shuchman M. Approving the vagus-nerve stimulator for depression. N Engl J Med. 2007;356(16):1604–7.
15. Koopman FA, Chavan SS, Miljko S, et al. Vagus nerve stimulation inhibits cytokine production and attenuates disease severity in rheumatoid arthritis. Proc Natl Acad Sci U S A. 2016;113(29):8284–9.
16. Sinniger V, Pellissier S, Fauvelle F, et al. A 12-month pilot study outcomes of vagus nerve stimulation in Crohn's disease. Neurogastroenterol Motil. 2020;32(10):e13911.
17. Tanaka S, Abe C, Abbott SBG et al. Vagus nerve stimulation activates two distinct neuroimmune circuits converging in the spleen to protect mice from kidney injury. Proc Natl Acad Sci U S A. 2021;118(12).
18. Inoue T, Abe C, Sung SS, et al. Vagus nerve stimulation mediates protection from kidney ischemia-reperfusion injury through alpha7nAChR+splenocytes. J Clin Invest. 2016;126(5):1939–52.
19. Lai Y, Deng J, Wang M, et al. Vagus nerve stimulation protects against acute liver injury induced by renal ischemia reperfusion via antioxidant stress and anti-inflammation. Biomed Pharmacother. 2019;117:109062.
20. Nakamura Y, Matsumoto H, Wu CH, et al. Alpha 7 nicotinic acetylcholine receptors signaling boosts cell-cell interactions in macrophages effecting anti-inflammatory and organ protection. Commun Biol. 2023;6(1):666.
21. Inoue T, Abe C, Kohro T, et al. Non-canonical cholinergic anti-inflammatory pathway-mediated activation of peritoneal macrophages induces Hes1 and blocks ischemia/reperfusion injury in the kidney. Kidney Int. 2019;95(3):563–76.
22. Tracey KJ. Physiology and immunology of the cholinergic antiinflammatory pathway. J Clin Invest. 2007;117(2):289–96.
23. Sabbah HN. Electrical vagus nerve stimulation for the treatment of chronic heart failure. Cleve Clin J Med. 2011;78(0 1):S24–9.
24. Domagala S, Domagala M, Chyla J, et al. Complications of electrotherapy - the dark side of treatment with cardiac implantable electronic devices. Postepy Kardiol Interwencyjnej. 2018;14(1):15–25.
25. Bao S, Lu Y, Zhang J, et al. Rapid improvement of heart repair in rats after myocardial infarction by precise magnetic stimulation on the vagus nerve with an injectable magnetic hydrogel. Nanoscale. 2023;15(7):3532–41.
26. Lu Y, Chen K, Zhao W, et al. Magnetic vagus nerve stimulation alleviates myocardial ischemia-reperfusion injury by the inhibition of pyroptosis through the M(2)AChR/OGDHL/ROS axis in rats. J Nanobiotechnol. 2023;21(1):421.
27. Williams EC, Coimbra R, Chan TW, et al. Precious cargo: modulation of the mesenteric lymph exosome payload after hemorrhagic shock. J Trauma Acute Care Surg. 2019;86(1):52–61.
28. Tkach M, Thery C. Communication by Extracellular vesicles: where we are and where we need to go. Cell. 2016;164(6):1226–32.
29. Martins-Marques T, Pinho MJ, Zuzarte M, et al. Presence of Cx43 in extracellular vesicles reduces the cardiotoxicity of the anti-tumour therapeutic approach with doxorubicin. J Extracell Vesicles. 2016;5:32538.
30. Jansen F, Nickenig G, Werner N. Extracellular vesicles in Cardiovascular Disease: potential applications in diagnosis, prognosis, and Epidemiology. Circ Res. 2017;120(10):1649–57.
31. Mori MA, Ludwig RG, Garcia-Martin R, et al. Extracellular miRNAs: from biomarkers to mediators of physiology and disease. Cell Metab. 2019;30(4):656–73.
32. Isaac R, Reis FCG, Ying W, et al. Exosomes as mediators of intercellular crosstalk in metabolism. Cell Metab. 2021;33(9):1744–62.
33. Yu Y, Chen M, Guo Q, et al. Human umbilical cord mesenchymal stem cell exosome-derived mir-874-3p targeting RIPK1/PGAM5 attenuates kidney tubular epithelial cell damage. Cell Mol Biol Lett. 2023;28(1):12.
34. Guo C, Dong G, Liang X, et al. Epigenetic regulation in AKI and kidney repair: mechanisms and therapeutic implications. Nat Rev Nephrol. 2019;15(4):220–39.
35. Shivdasani RA. MicroRNAs: regulators of gene expression and cell differentiation. Blood. 2006;108(12):3646–53.
36. Pan Z, Zhang M, Ma T, et al. Hydroxymethylation of microRNA-365-3p regulates nociceptive behaviors via Kcnh2. J Neurosci. 2016;36(9):2769–81.
37. Binenbaum Y, Fridman E, Yaari Z, et al. Transfer of miRNA in macrophage-derived Exosomes induces Drug Resistance in pancreatic adenocarcinoma. Cancer Res. 2018;78(18):5287–99.
38. Nguyen MA, Karunakaran D, Geoffrion M, et al. Extracellular vesicles secreted by Atherogenic Macrophages Transfer MicroRNA to Inhibit Cell Migration. Arterioscler Thromb Vasc Biol. 2018;38(1):49–63.
39. Schaefer E, Wu W, Mark C, et al. Intermittent hypoxia is a proinflammatory stimulus resulting in IL-6 expression and M1 macrophage polarization. Hepatol Commun. 2017;1(4):326–37.
40. Yuan Y, Yuan L, Yang J, et al. Autophagy-deficient macrophages exacerbate cisplatin-induced mitochondrial dysfunction and kidney injury via miR-195a-5p-SIRT3 axis. Nat Commun. 2024;15(1):4383.
41. Chen B, Sun J, Fan F, et al. Ferumoxytol of ultrahigh magnetization produced by hydrocooling and magnetically internal heating co-precipitation. Nanoscale. 2018;10(16):7369–76.
42. McCullough PA, Choi JP, Feghali GA, et al. Contrast-Induced Acute kidney Injury. J Am Coll Cardiol. 2016;68(13):1465–73.

43. Zhu X, Li S, Lin Q, et al. alphaKlotho protein has therapeutic activity in contrast-induced acute kidney injury by limiting NLRP3 inflammasome-mediated pyroptosis and promoting autophagy. Pharmacol Res. 2021;167:105531.
44. Balasubramanian S, Kota SK, Kuchroo VK, et al. TIM family proteins promote the lysosomal degradation of the nuclear receptor NUR77. Sci Signal. 2012;5(254):ra90.
45. Morcos R, Kucharik M, Bansal P, et al. Contrast-Induced Acute kidney Injury: review and practical update. Clin Med Insights Cardiol. 2019;13:1179546819878680.
46. Maioli M, Toso A, Leoncini M, et al. Bioimpedance-guided hydration for the Prevention of contrast-Induced kidney Injury: the HYDRA Study. J Am Coll Cardiol. 2018;71(25):2880–9.
47. Deng S, Zhang Y, Xin Y, et al. Vagus nerve stimulation attenuates acute kidney injury induced by hepatic ischemia/reperfusion injury in rats. Sci Rep. 2022;12(1):21662.
48. Wheless JW, Gienapp AJ, Ryvlin P. Vagus nerve stimulation (VNS) therapy update. Epilepsy Behav. 2018;88S:2–10.
49. Ben-Menachem E, Manon-Espaillat R, Ristanovic R, et al. Vagus nerve stimulation for treatment of partial seizures: 1. A controlled study of effect on seizures. First Int Vagus Nerve Stimulation Study Group Epilepsia. 1994;35(3):616–26.
50. Handforth A, DeGiorgio CM, Schachter SC, et al. Vagus nerve stimulation therapy for partial-onset seizures: a randomized active-control trial. Neurology. 1998;51(1):48–55.
51. Li R, Wang J, Yu X, et al. Enhancing the effects of transcranial magnetic stimulation with intravenously injected magnetic nanoparticles. Biomater Sci. 2019;7(6):2297–307.
52. Fang YT, Lin YT, Tseng WL, et al. Neuroimmunomodulation of vagus nerve stimulation and the therapeutic implications. Front Aging Neurosci. 2023;15:1173987.
53. Hilderman M, Bruchfeld A. The cholinergic anti-inflammatory pathway in chronic kidney disease-review and vagus nerve stimulation clinical pilot study. Nephrol Dial Transpl. 2020;35(11):1840–52.
54. Smolarz M, Widlak P. Serum exosomes and their miRNA Load-A potential biomarker of Lung Cancer. Cancers (Basel). 2021;13(6).
55. Lu L, Risch HA. Exosomes: potential for early detection in pancreatic cancer. Future Oncol. 2016;12(8):1081–90.
56. Gao L, Mei S, Zhang S, et al. Cardio-renal exosomes in myocardial infarction serum regulate Proangiogenic Paracrine Signaling in adipose mesenchymal stem cells. Theranostics. 2020;10(3):1060–73.
57. Zhang R, Guo J, Wang Y, et al. Prenatal bisphenol S exposure induces hepatic lipid deposition in male mice offspring through downregulation of adipose-derived exosomal miR-29a-3p. J Hazard Mater. 2023;453:131410.
58. Chen X, Guo J, Mahmoud S, et al. Regulatory roles of SP-A and exosomes in pneumonia-induced acute lung and kidney injuries. Front Immunol. 2023;14:1188023.
59. Pan T, Jia P, Chen N, et al. Delayed remote ischemic preconditioning ConfersRenoprotection against septic acute kidney Injury via Exosomal miR-21. Theranostics. 2019;9(2):405–23.
60. Li X, Xu H, Yi J, et al. miR-365 secreted from M2 macrophage-derived extracellular vesicles promotes pancreatic ductal adenocarcinoma progression through the BTG2/FAK/AKT axis. J Cell Mol Med. 2021;25(10):4671–83.
61. Zuo Z, Li Q, Zhou S et al. Berberine ameliorates contrast-induced acute kidney injury by regulating HDAC4-FoxO3a axis-induced autophagy: in vivo and in vitro. Phytother Res. 2023;37(5):1950-1961.
62. Liu X, Li Q, Sun L, et al. miR-30e-5p regulates autophagy and apoptosis by targeting Beclin1 involved in contrast-induced acute kidney Injury. Curr Med Chem. 2021;28(38):7974–84.
63. Rajawat Y, Hilioti Z, Bossis I. Autophagy: a target for retinoic acids. Autophagy. 2010;6(8):1224–6.
64. Zhang C, Liu XR, Cao YC, et al. Mammalian target of rapamycin/eukaryotic initiation factor 4F pathway regulates follicle growth and development of theca cells in mice. Reprod Fertil Dev. 2017;29(4):768–77.
65. Shu Q, Xu Y, Zhuang H, et al. Ras homolog enriched in the brain is linked to retinal ganglion cell apoptosis after light injury in rats. J Mol Neurosci. 2014;54(2):243–51.
66. Chen XB, Wang ZL, Yang QY et al. Diosgenin glucoside protects against spinal cord Injury by regulating autophagy and alleviating apoptosis. Int J Mol Sci. 2018;19(8).
67. Khuanjing T, Maneechote C, Ongnok B, et al. Vagus nerve stimulation and acetylcholinesterase inhibitor donepezil provide cardioprotection against trastuzumab-induced cardiotoxicity in rats by attenuating mitochondrial dysfunction. Biochem Pharmacol. 2023;217:115836.
68. Shinlapawittayatorn K, Chinda K, Palee S, et al. Vagus nerve stimulation initiated late during ischemia, but not reperfusion, exerts cardioprotection via amelioration of cardiac mitochondrial dysfunction. Heart Rhythm. 2014;11(12):2278–87.
69. Wang H, Yu M, Ochani M, et al. Nicotinic acetylcholine receptor alpha7 subunit is an essential regulator of inflammation. Nature. 2003;421(6921):384–8.
70. Rosso P, Iannitelli A, Pacitti F, et al. Vagus nerve stimulation and neurotrophins: a biological psychiatric perspective. Neurosci Biobehav Rev. 2020;113:338–53.
71. Gold MR, Van Veldhuisen DJ, Hauptman PJ, et al. Vagus nerve stimulation for the treatment of Heart failure: the INOVATE-HF Trial. J Am Coll Cardiol. 2016;68(2):149–58.
72. Zannad F, De Ferrari GM, Tuinenburg AE, et al. Chronic vagal stimulation for the treatment of low ejection fraction heart failure: results of the NEural Cardiac TherApy foR Heart failure (NECTAR-HF) randomized controlled trial. Eur Heart J. 2015;36(7):425–33.
73. Yano T, Itoh Y, Kubota T, et al. A prostacyclin analog prevents radiocontrast nephropathy via phosphorylation of cyclic AMP response element binding protein. Am J Pathol. 2005;166(5):1333–42.
74. Lu Y, Zhang J, Han B, et al. Extracellular vesicles DJ-1 derived from hypoxia-conditioned hMSCs alleviate cardiac hypertrophy by suppressing mitochondria dysfunction and preventing ATRAP degradation. Pharmacol Res. 2023;187:106607.
75. Ge X, Meng Q, Wei L, et al. Myocardial ischemia-reperfusion induced cardiac extracellular vesicles harbour proinflammatory features and aggravate heart injury. J Extracell Vesicles. 2021;10(4):e12072.
76. Catalano M, O'Driscoll L. Inhibiting extracellular vesicles formation and release: a review of EV inhibitors. J Extracell Vesicles. 2020;9(1):1703244.
77. Liu T, Fang Y, Liu S, et al. Limb ischemic preconditioning protects against contrast-induced acute kidney injury in rats via phosphorylation of GSK-3beta. Free Radic Biol Med. 2015;81:170–82.
78. Zhao P, Zhu Y, Sun L, et al. Circulating Exosomal Mir-1-3p from rats with myocardial infarction plays a protective effect on contrast-Induced Nephropathy via Targeting ATG13 and activating the AKT Signaling Pathway. Int J Biol Sci. 2021;17(4):972–85.
79. Sun L, Zhu W, Zhao P, et al. Long noncoding RNA UCA1 from hypoxia-conditioned hMSC-derived exosomes: a novel molecular target for cardioprotection through miR-873-5p/XIAP axis. Cell Death Dis. 2020;11(8):696.

Publisher's note